Int. J. Electrochem. Sci., 17 **(2022)** Article Number: 220760, doi: 10.20964/2022.07.66

International Journal of
ELECTROCHEMICAL
SCIENCE
www.electrochemsci.org

Under Deposit Corrosion of Low Alloy Steel in Saturated CO_2 Formation Water

Xuanpeng Li[1], *Xiaodong Wang*[2], *Xiaogang Chen*[2], *Wei Yuan*[2], *Zihan Chen*[1], *Peng Cui*[3], *Juntao Yuan*[1,*], *Anqing Fu*[1]

[1] State Key Laboratory for Performance and Structure Safety of Petroleum Tubular Goods and Equipment Materials of CNPC Tubular Goods Research Institute, Xi'an 710077, China
[2] Shenzhen Branch of CNOOC (China) Limited, Shenzhen 518000, China
[3] Dagang Oilfield Production Technology Research Institute, China National Petroleum Corporation, Tianjin 300280, China
[*]E-mail: yuanjt@cnpc.com.cn

Received: 8 November 2021 / *Accepted:* 27 December 2021 / *Published:* 6 June 2022

The corrosion behavior of L245N steel uncovered and covered with deposit in saturated CO_2 formation water was researched by using the surface morphology analysis and electrochemical measurements. The results delineated that the corrosion resistance of both the steel uncovered and covered with the deposit performed the same characteristics, which enhanced in the initial stage, and then decreased obviously. For the uncovered steel, the enhanced corrosion resistance due to the protection of the corrosion film, the reduced corrosion resistance resulted from the rupture of the corrosion film. Moreover, for the covered steel, the deposit could also protect the steel in the initial stage, then that promoted the formation of the occluded cell and accelerated the corrosion rate obviously.

Keywords: Deposit; Uncovered and covered; Corrosion resistance; Occluded cell; Corrosion rate

1. INTRODUCTION

Gathering and transportation line is an important link in the oil field. CO_2 corrosion isa failure mode causing in oil and gas production and transportation systems [1-6], resulting in the significant economic losses and accidents [7-9]. Under the combined effect of CO_2 and temperature, scaling phenomenon often occur in pipeline, leading to the serious corrosion of the inner wall of pipeline.

Intensive researches had conducted to investigate the corrosion of metal under sediments [10-17]. Pedserent et al. [18] studied the influence of galvanic current formed between the sediment-covered area and the sediment-free zone on the sediment corrosion and thought the sediment-covered area was used as the anode, the sediment-free area was the cathode. But the cause of corrosion was not explained. Reus [19] thought the addition of inhibitor might effectively inhibit corrosion of pipe under the sediments and the results indicated the inhibitors inhibited the corrosion well. This might be due to the low concentration of inhibitor. Pandarinathan [20] believed the presence of deposits might affect the inhibition performance of inhibitor. Many scholars had not only explored the corrosion mechanism and protection measures of metal with sediments, but also proposed a lot of advanced experimental devices [21-26].

In the past, the oxygen concentration cells were considered to be main cause of corrosion under deposits [27, 28]. However, the autocatalytic effect of blocked cells formed in metal covered by deposits under the condition of oxygen-without might be also a more important reason of corrosion with the continuous progresses of researches. Therefore, it had become the focus to study the corrosion mechanism of metal under sediments.

In order to avoid the influence of oxygen concentration cells, the experiments were carried out without oxygen. The corrosion resistance of L245N steel covered with and without deposits was measured by potentiodynamic polarization curves, electrochemical impedance spectra (EIS) and wire beam electrode (WBE) method in CO_2-saturated simulated oilfield produced water, the corrosion mechanism of L245N steel was also studied.

2. EXPERIMENTAL

2.1. Materials and solution

The materials were L245N steel. And the chemical compositions of L245N steel (wt. %) were: C ($\leq$ 0.28), Si ($\leq$ 0.40), Mn ($\leq$1.20), P ($\leq$ 0.035), S ($\leq$ 0.02), V ($\leq$ 0.06), NB ($\leq$ 0.01) and Fe balance. potentiodynamic polarization curve and EIS were carried out using the samples with 10 × 10 × 10 mm^3 . The specimens were sealed in epoxy resin and with an exposed area of 1.0 cm^2. Besides, for the WBE measurement, the WBE was obtained by placing L245N steel wires in a regular arrangement of 10 × 10 matrix (1 mm diameter) and embedding it in epoxy resin at 1 mm intervals. During the electrochemical measurements and WBE tests, the samples were ground to 2000 # SiC paper, then cleaned with deionized water, ethanol and dried.

Calcite (Calcium carbonate, $CaCO_3$) is one of the most common deposits. Therefore, the specimens coated with $CaCO_3$ were used to simulate the scale corrosion. The O-ring was first placed on the samples for electrochemical tests and WBE measurements, then the surface of samples is filled with wet $CaCO_3$ sludge and finally was dried in a stream of compressed hot air.

The test solution is simulating formation water and its chemical composition was listed in Table 1. The test solution was deoxygenated with N_2 gas for approximately 4 h and infused with CO_2 at a low flow rate. All temperature was maintained at 25 ± 1 °C during the tests.

Table 1. Composition of formation water from the oilfield.

Component	$CaCl_2$	NaCl	$MgCl_2$	KCl	K_2SO_4	$Ca(HCO_3)_2$	KI	KBr
Content (g/L)	35.52	168.32	7.21	9.16	0.36	0.85	0.0039	0.21

2.2. Immersion experiments

The immersion experiments for L245N steel under deposit were conducted in a 5L autoclave to research the corrosion rate of L245N steel in saturated CO_2 formation water The specimens were immediately taken out the autoclave and subsequently rinsed successively using deionized water and anhydrous ethanol when the immersion experiment was completed. According to ASTM standard G1-03 [29], the solution consists of nitric acid (100 mL; Density: 1.42 g/mL), hydrofluoric acid (20 mL; A solution consisting of 1.15 g/mL) and deionized water (880 mL), which was used to remove corrosion products from immersion test specimens at room temperature. After removing the corrosion products, the specimens were washed with deionized water and dried, and weighed again. The weight of this weighing is the final weight (W_1). Calculate the corrosion rate (V_c) in mm/a on the basis of weight loss date, which is given by Eq. (1).

$$V_c = \frac{87600(W_0 - W_1)}{t\rho A} \qquad (1)$$

where, W_0 and W_1 are the original and final weights of the specimen (g), respectively, t represents the immersion time (h), ρ represents the steel density (g/cm^3), and A is the specimens exposed surface area (cm^2).

2.3. Electrochemical measurement

All electrochemical measurements were carried out in a 1 L glass electrolytic cell using the electrochemical workstation (Zahner-Elektrik, Germany and CST520, China). The traditional three electrode system was applied to this study. Samples of steel with various treatment were used as working electrodes. A platinum sheet was used as the counter electrode. The reference electrode was an Ag/AgCl electrode, and its electrode potential is 0.222 V corresponding to standard hydrogen electrode (SHE) potentials. In this paper, all electrode potentials were converted to the potential relative to SHE. The polarization curve was obtained by scanning at the scanning rate of 0.333 mV/s from open circuit potential (OCP). EIS measurements were performed in the frequency range of 10^5-10^{-2} Hz by applying an sinusoidal signal with amplitude of 5 mV at OCP. The test results were fitted and analyzed using ZsimpWin software. The potential and current distributions of different specimen surfaces were studied by the WBE method. The wire beam electrode scanner was used for measuring the relative reference open-circuit potential and the short connection current of each metal wire, and the test was one by one. The input impedance was 1×10^{12} Ω, the maximum measurement potential and current range were ±5 V and ±20 mA, respectively. First scan the potential information of 100 lines, and then get according current information. Scanning between different wires requires an interval of 1.0 s, and it taken a total of 200 s for all electrodes to complete the test.

3. RESULTS

3.1. Weight loss analysis of L245N covered by deposit in saturated CO_2 formation water

To better research the corrosion rates of L245N steel uncovered and covered with deposits in the different time, the weight loss tests were measured. The corrosion rates determined by weight loss of L245N steel uncovered and covered with deposits exposed to saturated CO_2 formation water were shown in Figure 1. The corrosion rate of L245N steel with and without deposits decreased and then increased (Figure 1a). Moreover, the corrosion rate of L245N steel with deposits was much faster compared with the L245N steel uncovered by deposits (Figure 1a). The local corrosion of L245N steel covered by deposits is higher than that of L245 steel without deposits (Figure 1b).

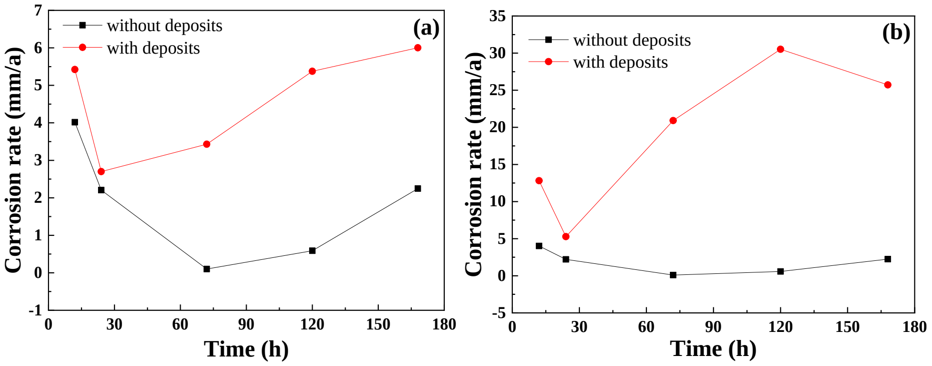

Figure 1. the corrosion rate (a) and local corrosion rate (b) of L245N steel uncovered and covered with deposits with the increasing of immersion time in saturated CO_2 formation water.

3.2. Electrochemical behavior of L245N covered by deposit in saturated CO_2 formation water

3.2.1. Potentiodynamic Polarization curves

The potentiodynamic polarization measurements were used for investigating the corrosion behavior of L245N steel uncovered and covered with deposits in saturated aqueous CO_2 environment. The polarization curves were shown in Figure 2. What's more, the corresponding test results were summarized in Table 2. The corrosion potential (E_{corr}) of L245N steel without deposits was higher than that of L245N steel with deposits, and the corrosion current density i_{corr} of L245 steel covered by deposits (2.16×10^{-5} A/cm^2) was 2.25 times than that of L245N steel not covered by sediments (5.96×10^{-6} A/cm^2), indicating the L245N steel covered with sediments was easier to corrosion and the degree of corrosion was more serious. This result agrees with Ref. [30-32].

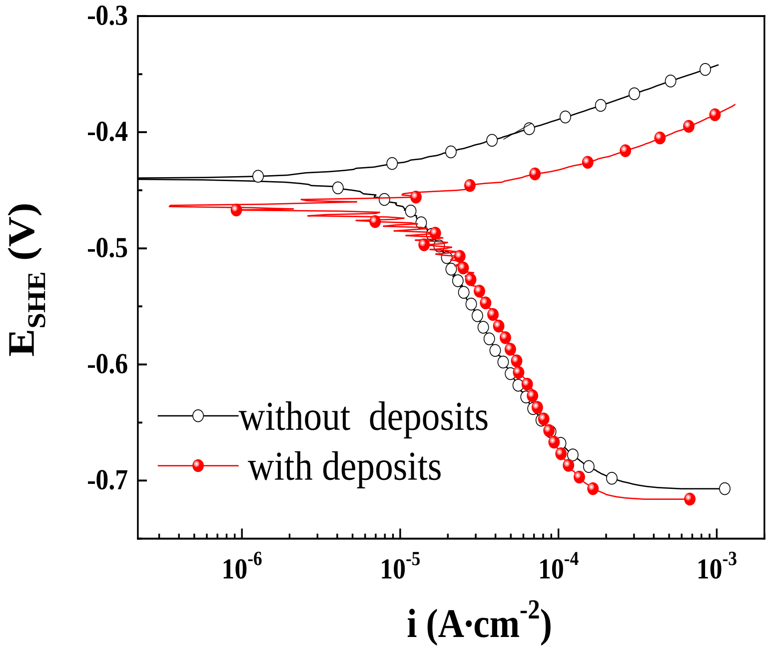

Figure 2. the potentiodynamic polarization curves of L245N steel uncovered and covered with deposits in saturated CO_2 formation water at 25℃.

Table 2. the E_{corr} and i_{corr} of L245N steel uncovered and covered with deposits in saturated CO_2 formation water.

	E_{corr} (V)	i_{corr} (A/cm^2)
L245N steel without deposits	-0.430	5.96×10^{-6}
L245N steel with deposits	-0.476	2.16×10^{-5}

3.2.2. EIS

Figures 3 and 4 illustrated the EIS of L245N steel uncovered with deposits with the different immersion time in saturated CO_2 formation water, respectively. It can be seen from the Bode plots and Nyquist plots of EIS that the capacitance loop radius and impedance modulus |Z| at low frequency ($|Z|_{0.01Hz}$) increased with the increase of immersion time within 0-12 hours, but decreased when the immersion time reached 24 hours. This was due to the corrosion product film was formed in the surface of L245N steel to prevent substrate from corrosion during the initial stage of immersion. In the later stage, the corrosion product film was destroyed and a large number of corrosive mediums penetrated into the surface of the L245N steel, resulting in the corrosion resistance decreased.

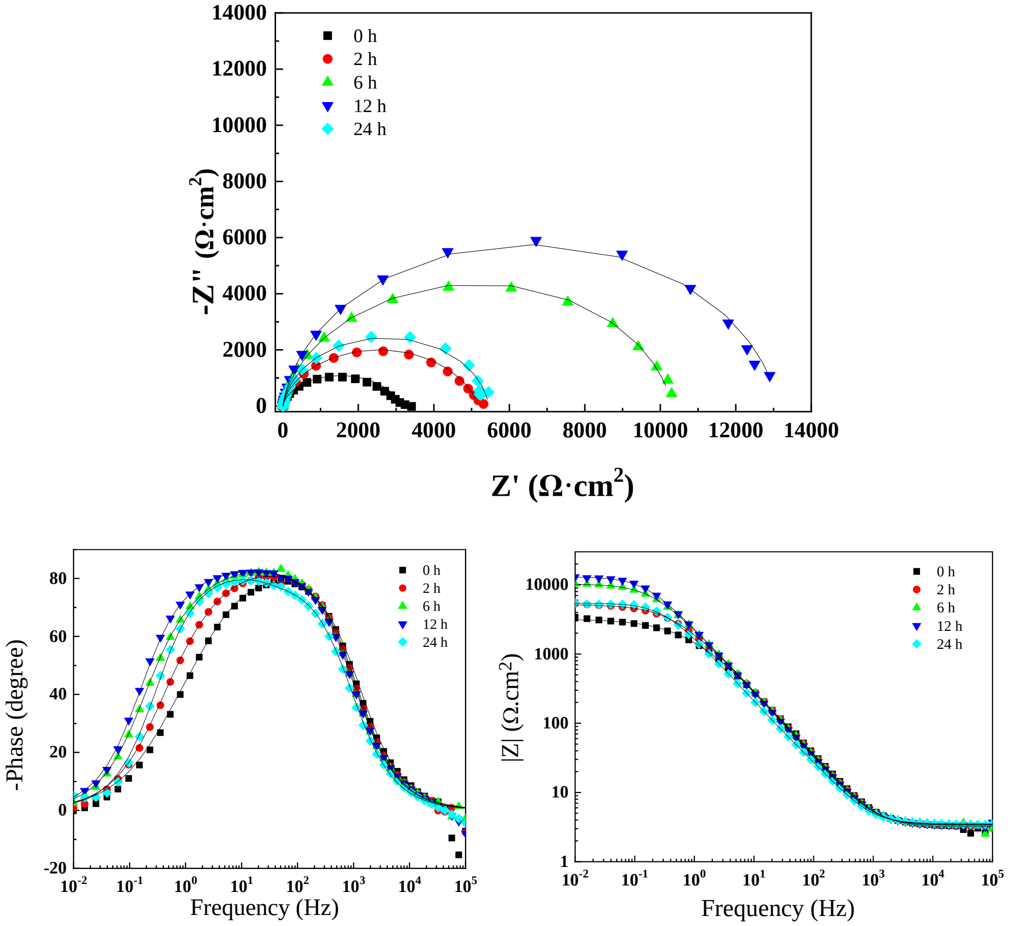

Figure 3. EIS of L245N steel uncovered with deposits with the increasing of immersion time (0-24 h) at the open circuit potential (OCP) in saturated CO_2 formation water at 25 ± 1 ℃.

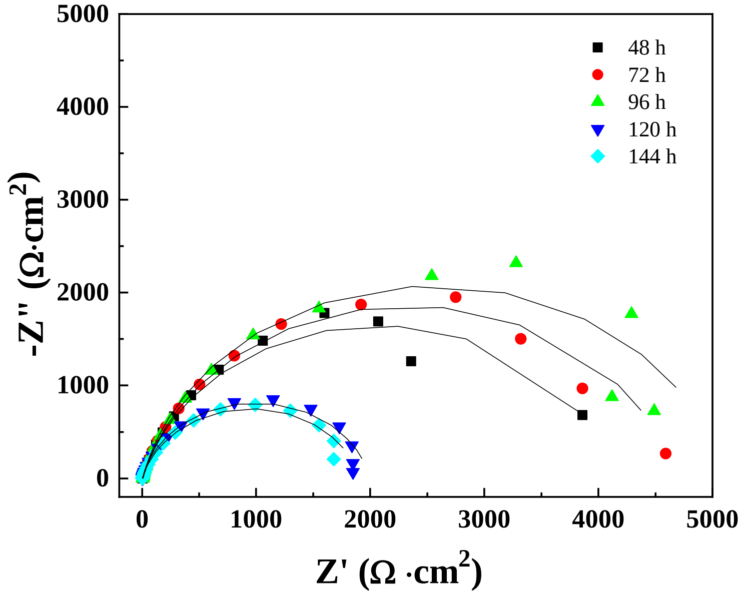

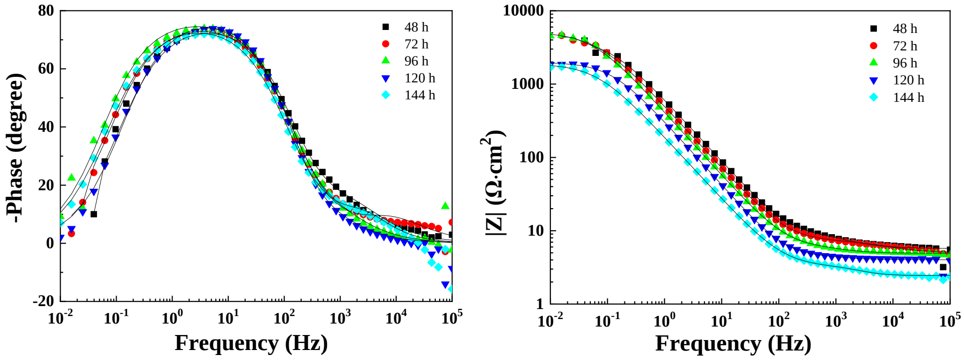

Figure 4. EIS of L245N steel uncovered with deposits with the increasing of immersion time (48-144 h) at the open circuit potential (OCP) in saturated CO_2 formation water at 25 ± 1 ℃.

Figures 5 and 6 showed the EIS of L245N steel covered with deposits with the increasing of immersion time. The capacitive loop diameter and $|Z|_{0.01Hz}$ increased in the early immersion. The reason for this phenomenon was that the sediment layer covers the surface of L245N steel and plays a protective effect. After 12 hours of immersion, the diameter of capacitive loop and $|Z|_{0.01Hz}$ decreased. With the extension of immersion time, the sediment layer covered the surface of L245N steel and formed an occluded area, made it difficult for Fe^{2+} and Fe^{3+} to diffuse out of the occluded area, leading to the residual metal cation in the occluded region. For maintaining the balance of positive and negative charge in the occluded area, anion will move to the block area, the hydrolysis of metal chloride acidifies the solution, which resulted in the L245N steel occur autocatalytic effect and the corrosion resistance decreased.

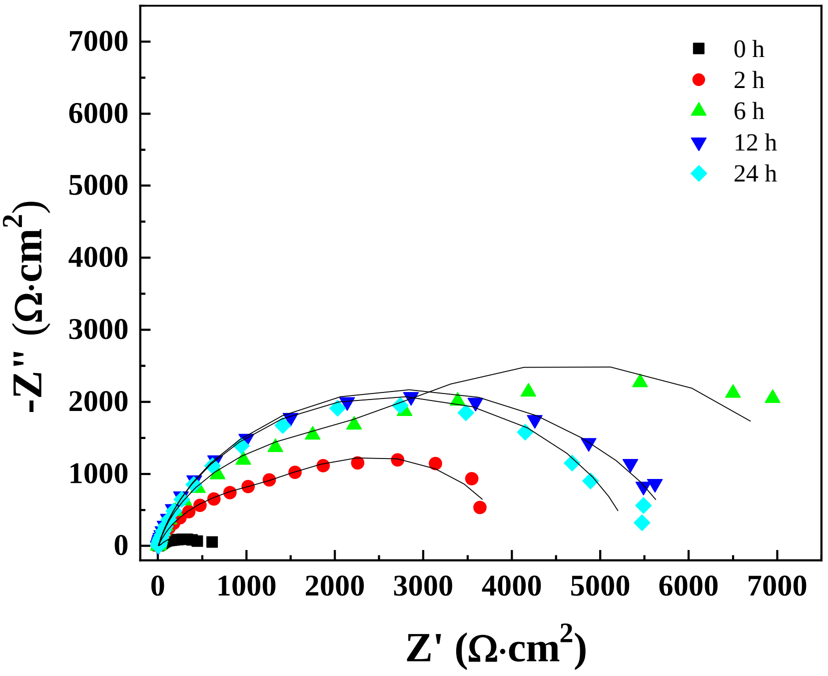

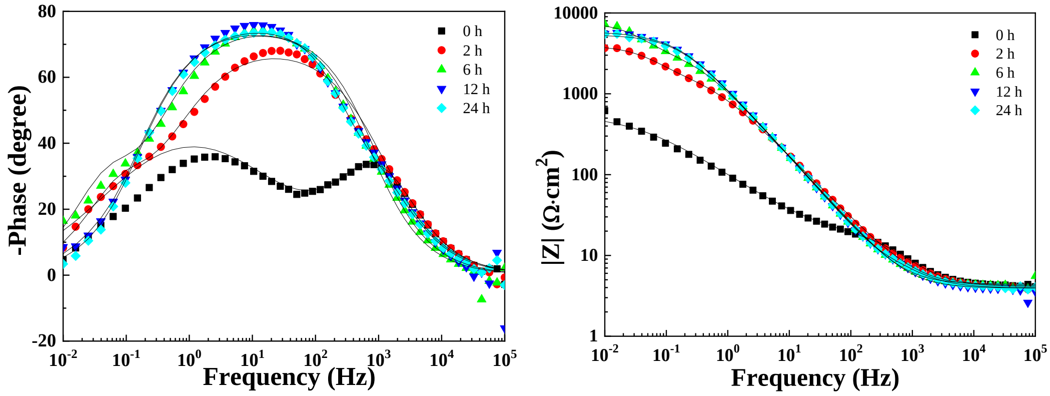

Figure 5. EIS of L245N steel covered with deposits with the increasing of immersion time (0-24 h) at the open circuit potential (OCP) in saturated CO_2 formation water at 25 ± 1 ℃.

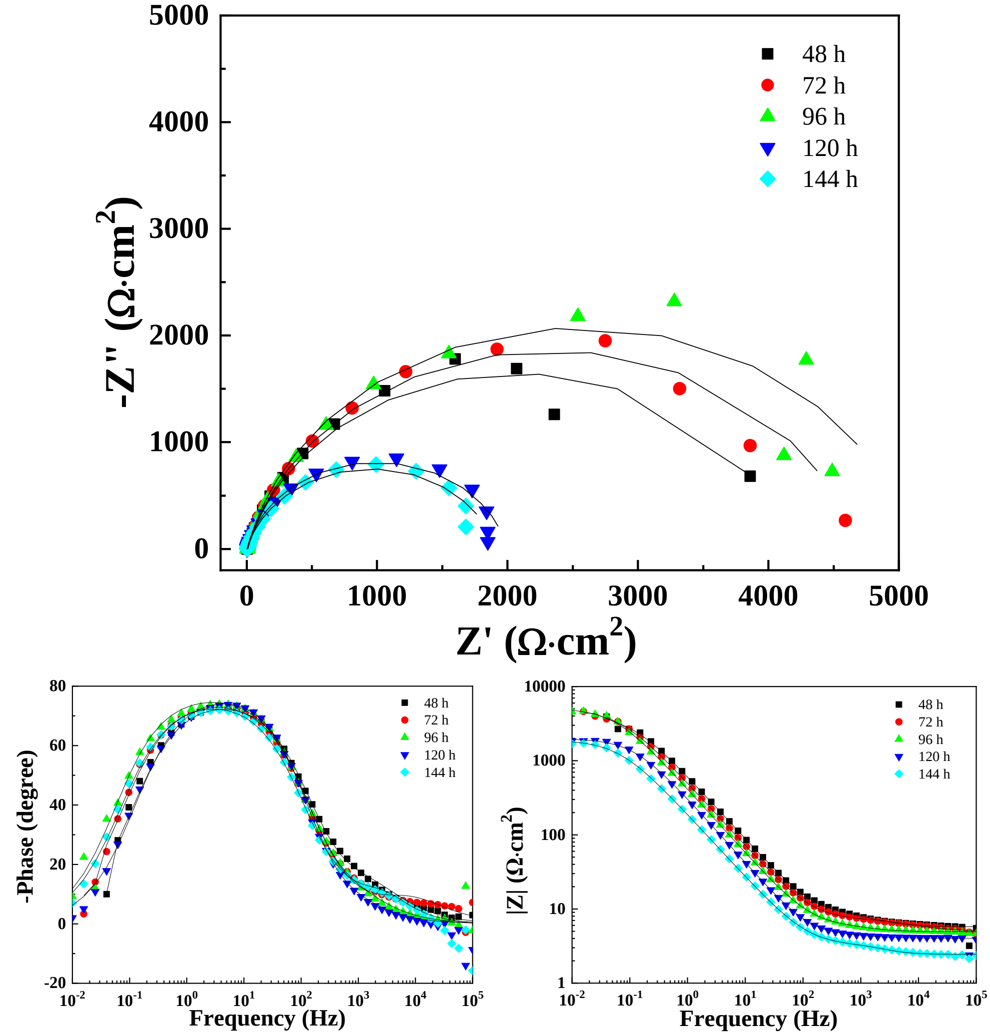

Figure 6. EIS of L245N steel covered with deposits with the increasing of immersion time (48-144 h) at the open circuit potential (OCP) in saturated CO_2 formation water at 25 ± 1 ℃.

The EIS was fitted using the equivalent circuit diagram in Figure 7. R_s is the solution resistance, R_f and R_{ct} are the corrosion product film resistance and charge transfer resistance respectively. Q is the constant phase element, Q_f and Q_{ct} represent the corrosion product film capacitance and the double layer capacitance respectively.

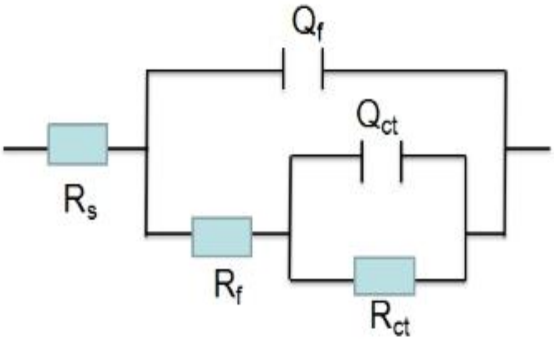

Figure 7. the equivalent circuit diagram of L245N steel uncovered and covered with deposits.

Based on the electrochemical parameters acquired by equivalent circuit fitting, the change of R_f and R_{ct} with the increasing of immersion time were illustrated in Figure 8. Regardless of whether the L245N steel was covered by deposits or not, R_f increased in the early stage, decreased after 24 h and finally reached a relatively stable value. The maximum value of R_f of L245N steel uncovered with deposits was much larger than that of L245N steel covered with, indicating that the sediments-covered L245N steel had a relatively stronger corrosion tendency even at the time point. Producing this phenomenon is because both corrosion products and deposits of L245N steel could protect the substrate in the early stages of immersion. Over time, the autocatalysis of blocked cells occurred in the L245N steel with and without deposits, making the R_f values reduce.

The R_{ct} of L245N steel covered by deposits increased in the early immersion stage, remained stable in the middle and decreased slightly after 96 h (Figure 8b). The deposition layer of L245N steel could act as the protective film before 24 h, enhancing the corrosion resistance of substrate. The autocatalytic effect of blocked cells and the protective effect of deposition layer reached a balance in the middle of immersion (24-96 h). With the augmentation of the autocatalytic effect, the charge transfer resistance became smaller after 96 h. The R_{ct} of L245N steel covered by deposits was smaller than that of L245N steel uncovered with deposits, indicating the deposition layer was more likely to deteriorate the corrosion resistance of substrate and the tendency of corrosion was stronger. This is also consistent with the potentiodynamic polarization curves.

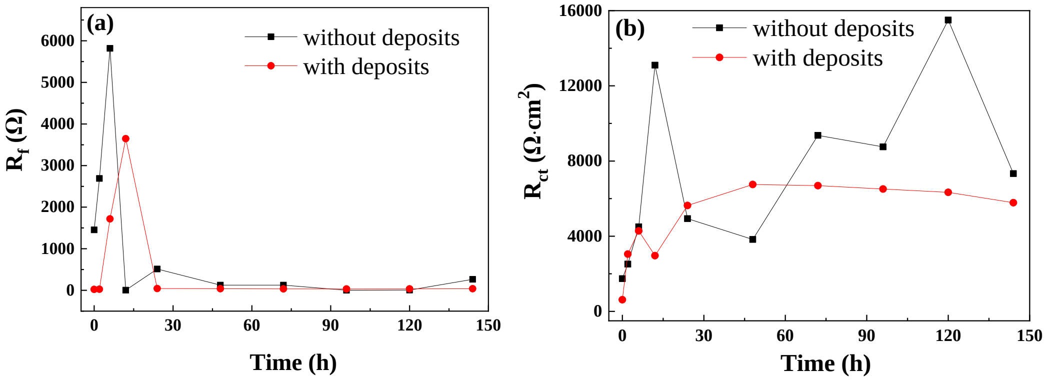

Figure 8. the R_f (a) and R_{ct} (b) of L245N steel uncovered and covered with deposits with the increasing of immersion time.

3.3. Surface morphology observation

Figure 9 showed the macrographs of L245N steel covered and uncovered with deposits after immersed 144 h in the saturated CO_2 formation water. The surface of L245N steel without sediment cover was only slightly corroded. However, most of the surface deposited-covered L245N steel was covered by corrosion products, especially the sediments-covered area (the inner area of red circle in figure), presenting a relatively uniform corrosion morphology. The corrosion of L245N steel covered by deposits was more serious than that of L245N steel uncovered with deposits.

Figure 10 showed the photos of corrosion microscopic morphology of bare L245N steel matrix and L245N steel covered by sediment after immersed 144 h in the saturated CO_2 formation water. The surface of the deposited-covered sample had corrosion pits of various sizes, while the other sample only had few corrosion pits. The result indicated the coating of deposits promoted the corrosion of L245N steel. Wang [33] also reported this result.

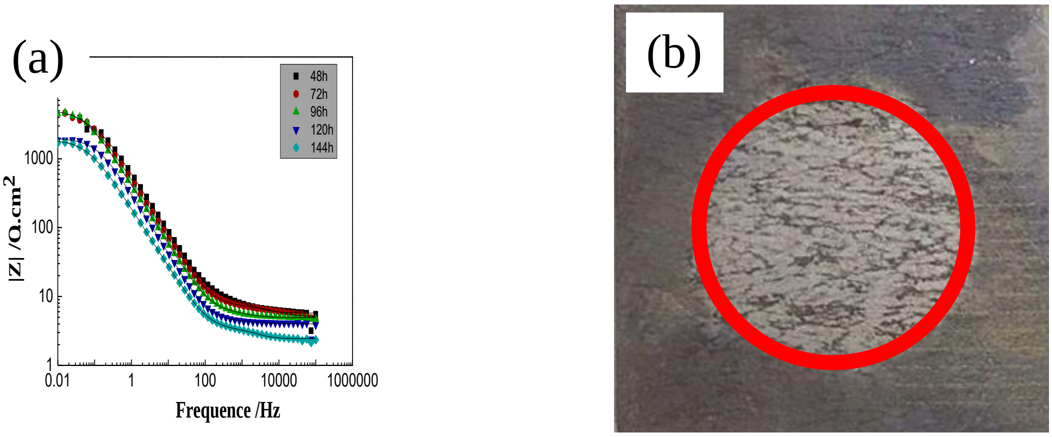

Figure 9. the macroscopic morphology of L245N steel uncovered with deposits (a) and covered with deposits (b) after immersed 144 h in saturated CO_2 formation water.

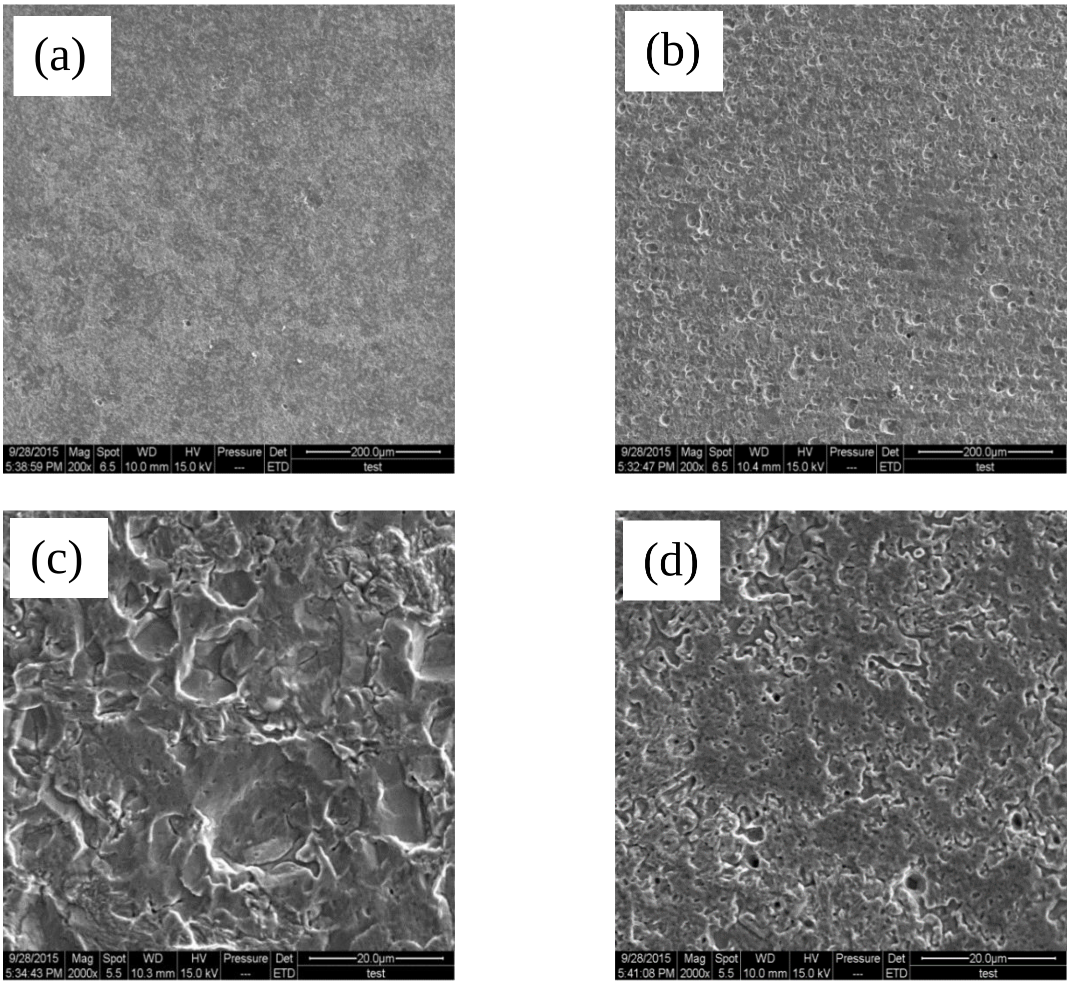

Figure 10. the microscopic morphology of L245N steel uncovered with deposits (a)(c), and covered with deposits (b)(d) after immersed 144 h in saturated CO_2 formation water.

4. DISCUSSION

The distribution of potential and current of the L245N steel uncovered with deposit for 0 h, 2 h, 6 h, 12 h, 24 h, 48 h, 72 h, 96 h, 120 h, 144 h was shown in Figure 11, respectively. (A)-(J) are the distribution of potential and (a)-(j) are the distribution of current. It shows that the corrosion potential showed that the corrosion potential shifted from about -670 mV to about -700 mV, while the galvanic current stabilized at about 2h, generally maintaining at about 0.7×10^{-3}mA. According to the distribution characteristics of potential and current, it can be determined that the corrosion occurs uniformly. Thus, the corrosion of the sample without deposit is slightly uniform, which in accordance with the polarization curve, EIS and surface corrosion morphology observation. Indicating that the corrosion products slightly enhance the corrosion resistance of the matrix at an incipient stage, then the product film destroyed and the corrosion resistance of the matrix decreased.

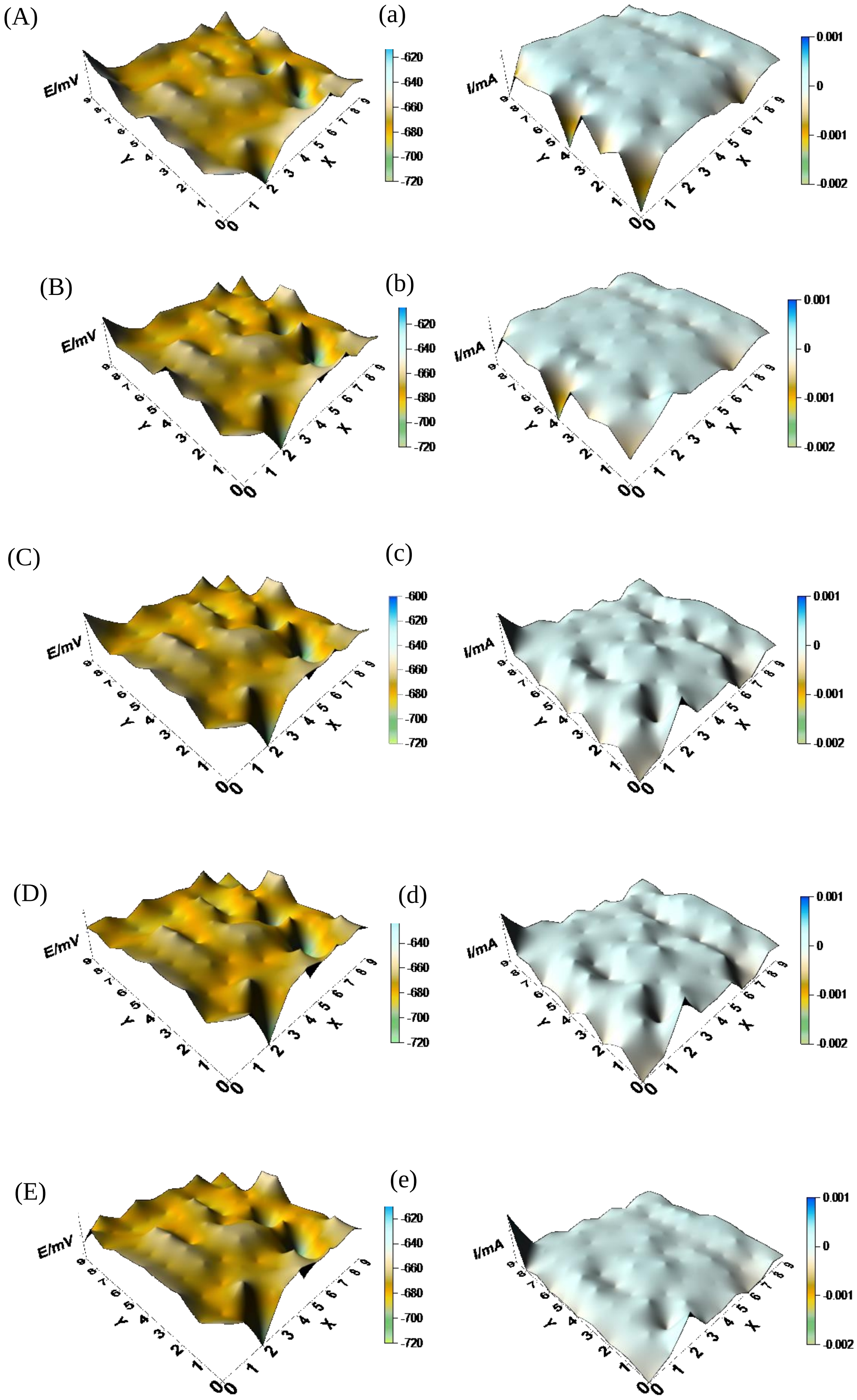
(A)
E/mV
X
Y
-620
-640
-660
-680
-700
-720
(a)
I/mA
X
Y
0.001
0
-0.001
-0.002
(B)
E/mV
-620
-640
-660
-680
-700
-720
(b)
I/mA
0.001
0
-0.001
-0.002
(C)
E/mV
-600
-620
-640
-660
-680
-700
-720
(c)
I/mA
0.001
0
-0.001
-0.002
(D)
E/mV
-640
-660
-680
-700
-720
(d)
I/mA
0.001
0
-0.001
-0.002
(E)
E/mV
-620
-640
-660
-680
-700
-720
(e)
I/mA
0.001
0
-0.001
-0.002

(F)

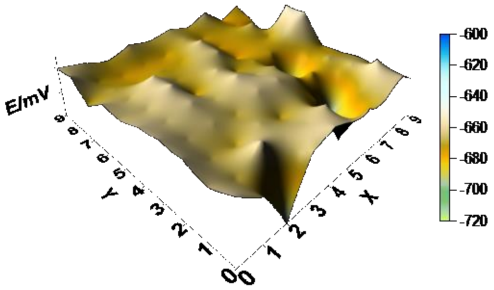
E/mV
Y
X
0
1
2
3
4
5
6
7
8
9
-600
-620
-640
-660
-680
-700
-720

(f)

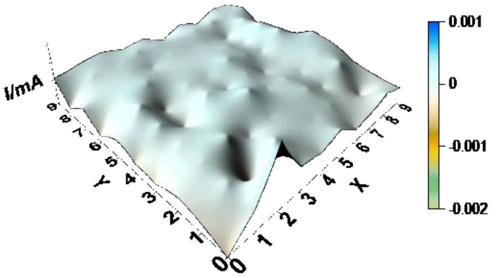
I/mA
Y
X
0
1
2
3
4
5
6
7
8
9
0.001
0
-0.001
-0.002

(G)

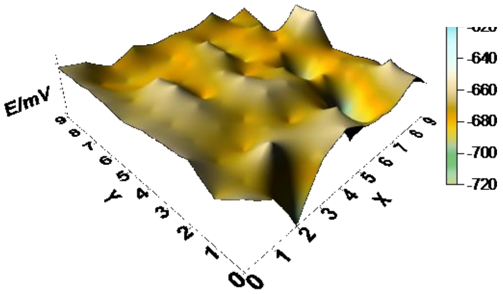
E/mV
Y
X
0
1
2
3
4
5
6
7
8
9
-640
-660
-680
-700
-720

(g)

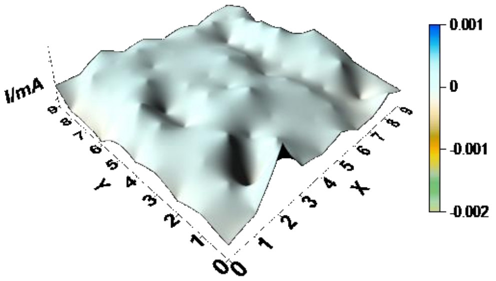
I/mA
Y
X
0
1
2
3
4
5
6
7
8
9
0.001
0
-0.001
-0.002

(H)

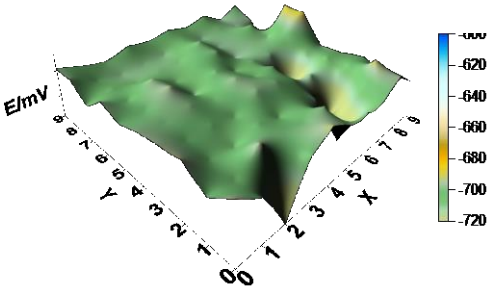
E/mV
Y
X
0
1
2
3
4
5
6
7
8
9
-620
-640
-660
-680
-700
-720

（h）

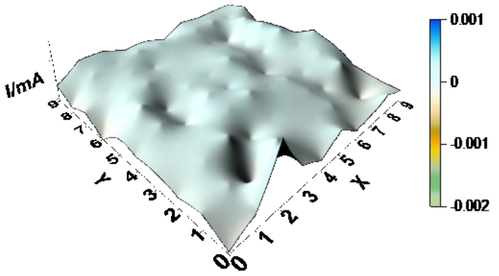
I/mA
Y
X
0
1
2
3
4
5
6
7
8
9
0.001
0
-0.001
-0.002

（I）

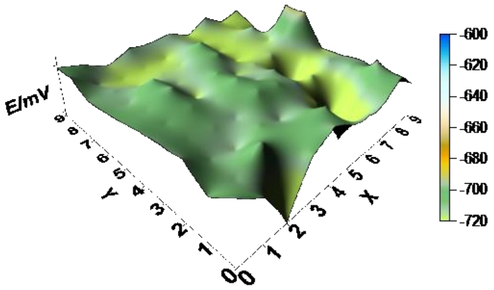
E/mV
Y
X
0
1
2
3
4
5
6
7
8
9
-600
-620
-640
-660
-680
-700
-720

（i）

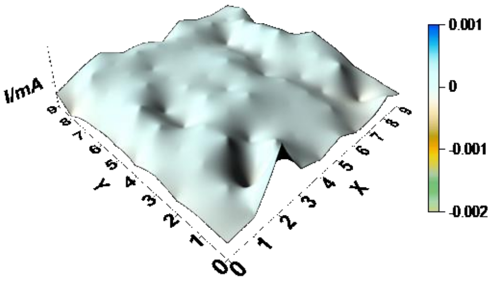
I/mA
Y
X
0
1
2
3
4
5
6
7
8
9
0.001
0
-0.001
-0.002

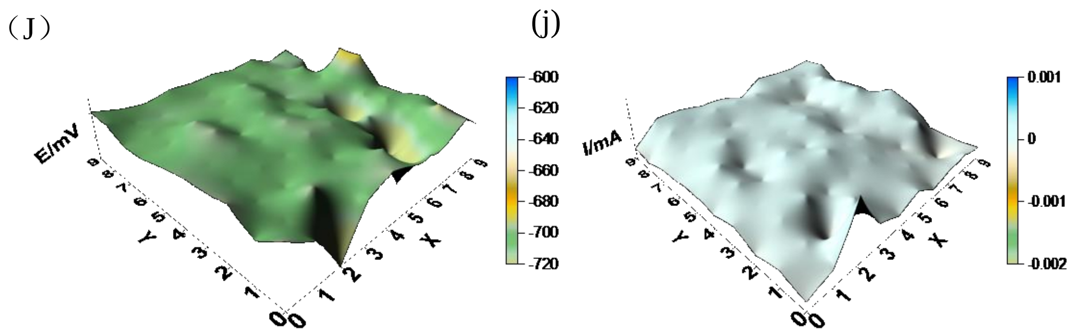

Figure 11. The distribution of potential and current over time of the L245N steel uncovered with deposits. The distribution of potential (A)-(J) and the distribution of current (a)-(j) for 0 h, 2 h, 6 h, 12 h, 24 h, 48 h, 72 h, 96 h, 120 h, 144 h respectively.

The distribution of potential and current of the L245N steel covered with deposits for 0 h, ,2 h,, 6 h, 12 h, 24 h, 48 h, 72 h, 96 h, 120 h, 144 h was shown in Figure 12, respectively. (A)-(J) are the distribution of potential and (a)-(j) are the distribution of current. It shows that the corrosion current of the covered area is positive and the uncovered area is negative in the initial period. After immersion for12 h, the corrosion current of the covered area is gradually increased, finally the whole electrode corrosion current remains at around 0.001 mA. This phenomenon coincided with the report of Song [34].

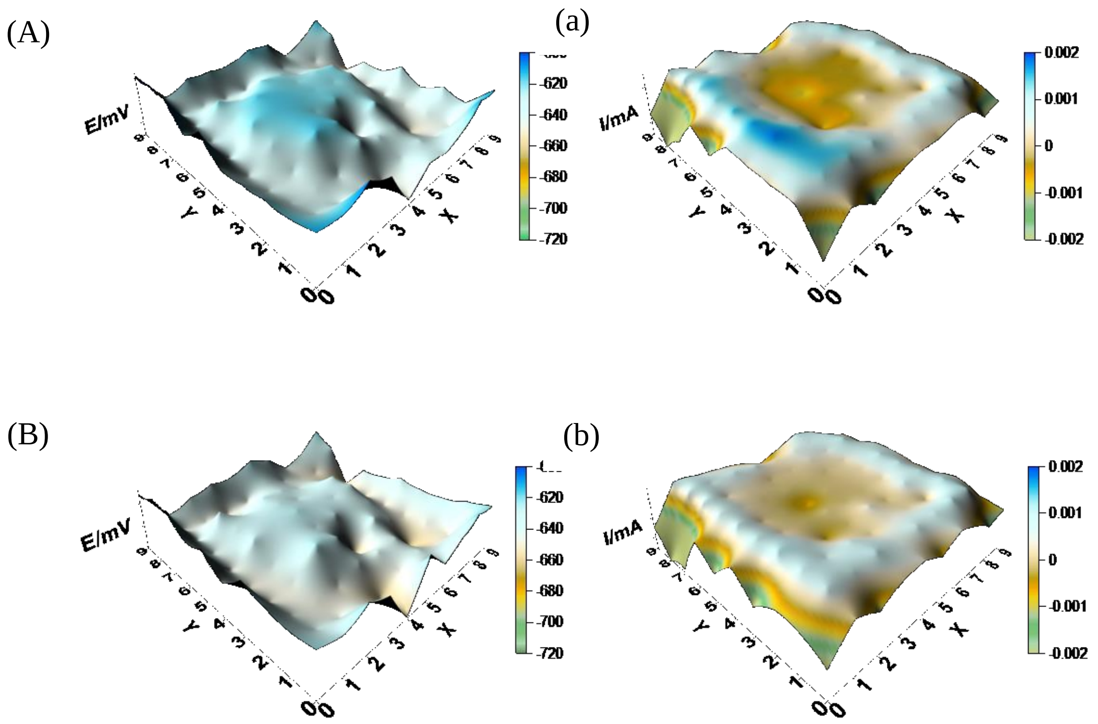

(C)

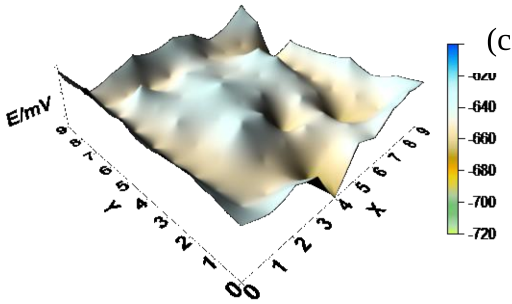
E/mV
X
Y
0 1 2 3 4 5 6 7 8 9
0 1 2 3 4 5 6 7 8 9
-620
-640
-660
-680
-700
-720

(c)

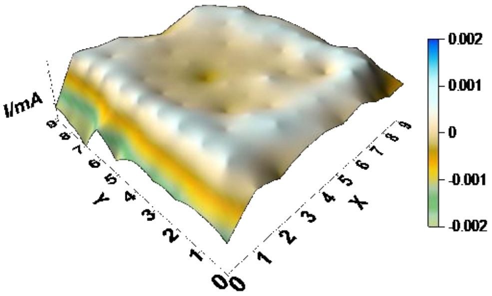
I/mA
X
Y
0 1 2 3 4 5 6 7 8 9
0 1 2 3 4 5 6 7 8 9
0.002
0.001
0
-0.001
-0.002

(D)

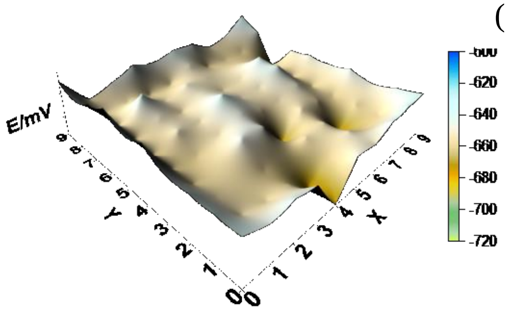
E/mV
X
Y
0 1 2 3 4 5 6 7 8 9
0 1 2 3 4 5 6 7 8 9
-600
-620
-640
-660
-680
-700
-720

(d)

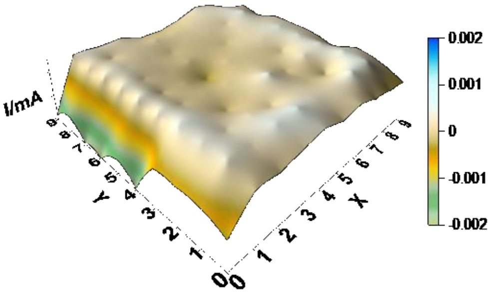
I/mA
X
Y
0 1 2 3 4 5 6 7 8 9
0 1 2 3 4 5 6 7 8 9
0.002
0.001
0
-0.001
-0.002

(E)

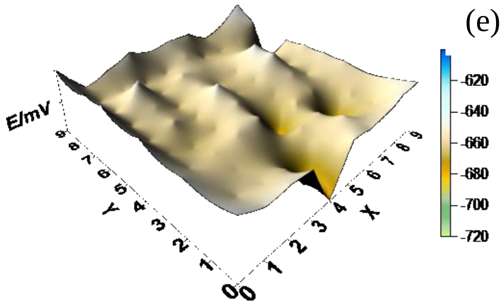
E/mV
X
Y
0 1 2 3 4 5 6 7 8 9
0 1 2 3 4 5 6 7 8 9
-620
-640
-660
-680
-700
-720

(e)

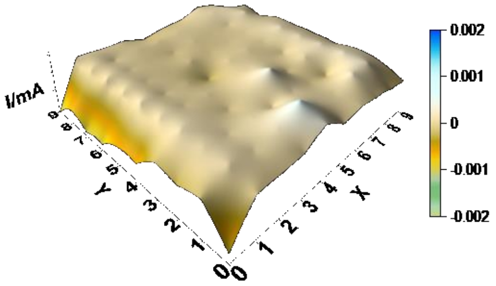
I/mA
X
Y
0 1 2 3 4 5 6 7 8 9
0 1 2 3 4 5 6 7 8 9
0.002
0.001
0
-0.001
-0.002

(F)

(f)

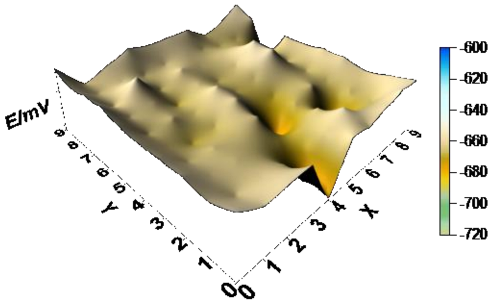
E/mV
X
Y
0 1 2 3 4 5 6 7 8 9
0 1 2 3 4 5 6 7 8 9
-600
-620
-640
-660
-680
-700
-720

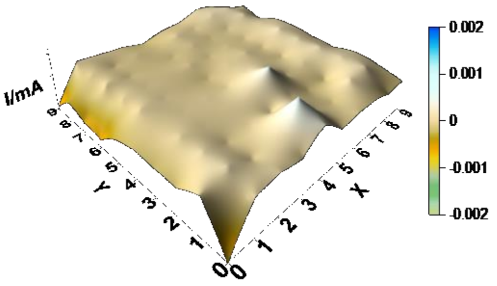
I/mA
X
Y
0 1 2 3 4 5 6 7 8 9
0 1 2 3 4 5 6 7 8 9
0.002
0.001
0
-0.001
-0.002

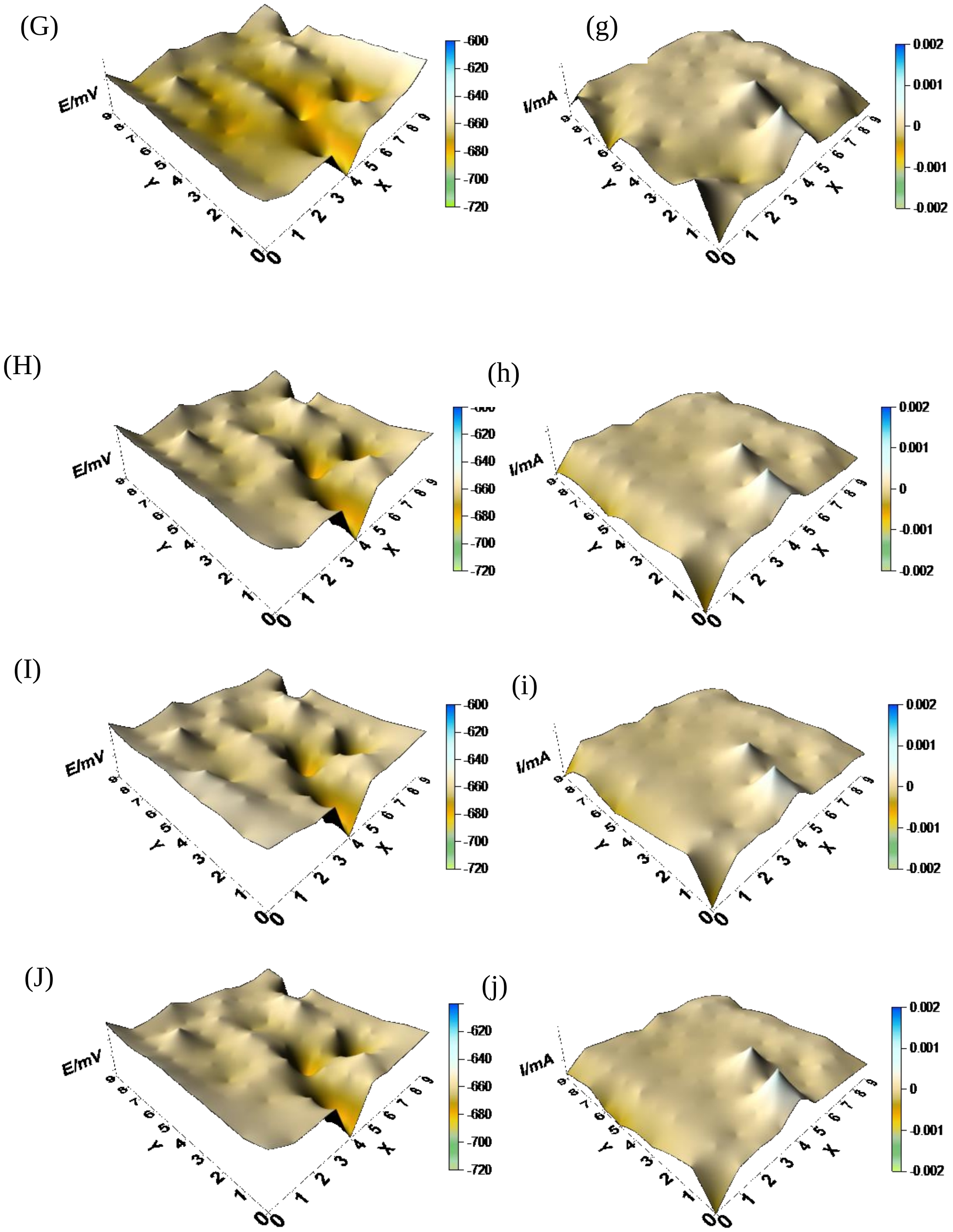

Figure 12. The distribution of potential and current over time of the L245N steel covered with deposits. The distribution of potential (A)-(J) and the distribution of current (a)-(j) for 0 h, 2 h, 6 h, 12 h, 24 h, 48 h, 72 h, 96 h, 120 h, 144 h respectively.

The corrosion potential is around 20 mV higher than the uncovered steel. It shows superior corrosion resistant in the earlier period. After immersion for 12 h, an amount of cation accumulated beneath the deposit. Then a large number of Cl^- was attracted. Thus, the occluded cell and accelerated the corrosion rate obviously. Therefore, it can see from the current distribution of wire beam electrode central area covered by deposit is relatively high, further illustrate the corrosion under the deposit is much more serious.

5. CONCLUSION

(1) When the L245N steel uncovered with the deposit, the corrosion resistance enhanced in the initial stage, and then decreased obviously. The above characteristics was due to the coverage of the corrosion scales film in the initial period. Followed by, the destruction of the corrosion scale film, and uniform corrosion accelerated.

(2) When the L245N steel covered with the deposit, the deposit protects the substrate in the initial stage. Latterly, the corrosion potential of L245N steel decreases by 30 mV and the corrosion current increases by about 2.25 times, forming an occluded cell under the deposit and causing serious corrosion of the steel due to the autocatalytic effect.

ACKNOWLEDGEMENTS
The authors wish to acknowledge the financial support of Basic research and strategic reserve technology research fund project of CNPC (2020D-5008(2020Z-08)), the National Natural Science Foundation of China (NO. U1460202, 2017004), Ningbo Science and Technology Innovation 2025 Major Special Project (2020Z108), Innovation Capability Support Program of Shaanxi (2019TD-038), and Innovation Capability Support Program of Shaanxi (2020KJXX-063), Scientific Research and Technology Development Project of Petrochina (2021ZZ01-04), Opening project fund of Materials Service Safety Assessment Facilities (MSAF-2020).

References

1. S. Li, J. Du, P. Guo, L. Sun and W. Yan, *Nat. Gas Ind.,* 27 (2007) 137.
2. M.M. Salama, *Corrosion*, 2000, NACE-00080.
3. G.A. Zhang and Y.F. Cheng, *Corros. Sci.,* 52 (2010) 2716-2724.
4. S. Nesic, *Corros. Sci.,* 49 (2007) 4308-4338.
5. R.M. Moreira, C.V. Franco, C.J.B.M. Joia, S. Giordana and O.R. Mattos, *Corros. Sci.,* 46 (2004) 2987-3003.
6. J. Banaś, U. Lelek-Borkowska, B. Mazurkiewicz and W. Solarski, *Electrochim. Acta.,* 52 (2007) 5704-5714.
7. L. Zeng, G.A. Zhang, X.P. Guo and C.W. Chai, *Corros. Sci.,* 90 (2015) 202-215.
8. G.A. Zhang, Y. Zeng, X.P. Guo, F. Jing and D.Y. Chen, *Corros. Sci.,* 65 (2012) 37-47.
9. H. Liu, T. Gu, G. Zhang, W. Wang, S. Dong, Y. Cheng and H. Liu, *Corros. Sci.,* 105 (2016) 149-160.
10. X. Wang and Robert E, *J. Loss Prev. Process Ind.,* 45 (2017) 29-42.
11. Y. Liu and E. Asselin, *J. Electrochem. Soc.,* 168 (2021) 071512.
12. E.M. Suarez, L.L. Machuca, B. Kinsella and K. Lepkova, *Corrosion,* 75 (2019) 1118-1127.
13. L. Pang, Z. Wang, W. Emori and Y. Zheng, *J. Mater. Eng. Perform.,* 2021, (30) 7552-7563.
14. Laura L. Machuca, K. Lepkova and A. Petroski, *Corros. Sci.,* 129 (2017) 16-25.
15. J.L. Crolet, *J. Mater. Sci.,* 28 (1993) 2589-2606.
16. C.M. Menendez, V. Jovancicevic and S. Ramachandran, *Corrosion,* 69 (2013) 145-156.
17. L. Pang, Z.B. Wang, M. H. Lu, Y. Lue, X. Liu and Y.G. Zheng, *Corros. Sci.,* 192 (2021) 109841.

18. A. Pedersen, K. Bilkova and E. Gulbrandsen, *Corrosion*, 2008, NACE-08632.
19. H. De Reus, L.J. A. Hendriksen and M. Wilms, *Corrosion*, 2005, NACE-05288.
20. V. Pandarinathan, K. Lepková, S.I. Bailey and R. Gubner, *Corros. Sci.,* 72 (2013) 108-117.
21. J.P. Smith, I. Gilbert and R. Kidder, *Corrosion*, 2001, NACE-01029.
22. W. Durnie, M. Gough and H. De Reus, *Corrosion*, 2005, NACE-05290.
23. Y. Tan, *Corrosion,* 54 (1998) 403-413.
24. Y. Tan, *J. Electrochem. Soc.,* 156 (2009) C195-C208.
25. W.Y. Mok, A. Jenkins and S.R. Keenan, *Corrosion*, 2005, NACE-05289.
26. K. Fushimi, A. Naganuma, K. Azumi and Y. Kawahara, *Corros. Sci.,* 50 (2008) 903-911.
27. G. Wu, K.L. More, C.M. Johnston, *Science,* 332 (2011) 443-447.
28. ASTM. Standard G1-03, ASTM International, West Conshohocken, PA, 2003.
29. L. Pang, Z. Wang, W. Emori and Y. Zheng, *J. Mater. Eng. Perform.,* 30 (2021) 7552-7563.
30. L. Pang, Z.B. Wang, M.H. Lu, Y. Lu, X. Liu and Y.G. Zheng, *Corros. Sci.,* 192 (2021) 109841.
31. L.L. Machuca, K. Lepkova and A. Petroski, *Corros. Sci.,* 129 (2017) 16-25.
32. X. Wang, R.E. Melchers, *J. Loss Prev. Process Ind.,* 45 (2017) 29-42.
33. Q. Cheng, B. Tao, L. Song, W. Zhang, X. Liu, W. Li, B. Hou and Q. Liu, *Corros. Sci.,* 111 (2016) 61-71.

© 2022 The Authors. Published by ESG (www.electrochemsci.org). This article is an open access article distributed under the terms and conditions of the Creative Commons Attribution license (http://creativecommons.org/licenses/by/4.0/).